Proceedings of
1999 ASME Turbo Expo: Land, Sea & Air
June7-10, Indianapolis, Indiana, USA

GT1999-0000

Degradation of Silicon Nitrides In High Pressure, Moisture Rich Environments

M. K. Ferber and H. T. Lin
Oak Ridge National Laboratory
Oak Ridge, TN

V. Parthasarathy and W. Brentnall
Solar Turbines
San Diego, CA

ABSTRACT

This paper provides a review of a recent study undertaken to examine the long-term reliability of silicon nitride and silicon carbide ceramics exposed to a representative gas turbine environment. A typical test exposure consisted of 500 hours at 1204°C and 1.5 atm of water vapor carried in an air environment at 10 atm of total pressure. Following each exposure specimens were weighed, measured, and then sectioned for optical and scanning electron microscopy. The total exposure duration was 1500 h for the silicon nitride and 2500 h for the silicon carbide.

INTRODUCTION

High performance silicon nitride and silicon carbide ceramics are leading candidates for use as high-temperature, structural components in advanced gas turbines [1-5]. These materials offer the following advantages over their metallic counterparts: (1) low density, (2) refractoriness, (3) adequate short-term strength, (4) good corrosion and oxidation resistance at intermediate to high oxygen partial pressures, and (5) their shape fabrication technology is fairly well established.

The gas turbine components, where ceramics could be inserted, include combustors, transition sections, hot gas ducts, vanes, and turbine blades. All but turbine blades are classified as stationary components. The materials for the stationary component require moderate hot strength, good thermal shock resistance, and shape stability. The rotating turbine blades call for higher strength materials and tolerance to impact. These components must also operate reliably for extended periods (>30,000 h for industrial gas turbines).

A major barrier to the utilization of structural ceramics as components in advanced heat engines is the uncertainty in the long-term mechanical reliability. Efforts to characterize the long-term mechanical reliability of monolithic ceramics for gas turbine applications have been underway in several laboratories in the United States including National Institute of Standards and Technology [1-4], University of Dayton. The SA SiC is a sintered silicon carbide which

*Research sponsored by U. S. Department of Energy's Office of Energy's Office of Energy Efficiency and Renewable Energy (Office of Industrial Technologies and Office of Fossil Energy (Morgantown Energy Technology Center) for the Advanced Turbine Systems Program, under contract DE-AC05-96OR22464 with Lockheed Martin Energy Research Corporation.

is fabricated in the green-state by injection molding. Small amounts of carbon and boron Research Institute [5, 6], and Oak Ridge National Laboratory [7-14]. The primary focus has been on measuring creep and stress rupture behavior. Table 1 provides a partial listing of the material systems that have been evaluated over the last ten years are added to assist the densification during sintering. Post-sinter hot isostatic pressing (HIPing) is also used to improve density and reduce defect size. The microstructure of this material typically consists of α silicon carbide grains ranging in size from 2 to 8 µm.

GN10, PY6, NT154, AND NT164 are fabricated by HIPing silicon nitride containing small amount of additives (primarily Y_2O_3). The resulting microstructures generally consist of both equiaxed and elongated silicon nitride grains separated by a Y-Si-O-N based intergranular phase. The exact composition of this phase depends upon the HIP conditions.

The HIPed silicon nitrides described above are no longer commercially available. In part this is due to the rather higher cost associated with the HIP process as compared to gas pressure sintering. There is also some question as to ability of the HIP process to be scaled up high volume manufacturing of ceramic components.

The SN88, AS800, SN253, and SN281/282 silicon nitrides are classified as self reinforced materials. Typical sintering aids include Y_2O_3 and Yb_2O_3.

Figure 1 through 2 illustrate typical stress rupture curves obtained for the SA SiC and SN88, respectively. These data were generated using the button-head specimen discussed in Reference 15. Representative data for the other materials listed in Table 1 can be found in the references cited at the beginning of this section.

One of the key limitations of the stress rupture curves described above is that they reflect the behavior of the material in air at ambient pressure. Unfortunately, the gas turbine environment includes water vapor at pressures in excess of 1 atmosphere. For a given temperature, oxidation of both silicon nitride and silicon carbide is increased by (1) the replacement of oxygen by water vapor and (2) an increase in the pressure of the oxidant. In addition, the high velocities and presence of water in the environment can lead to the volatilization of the normally protective silica layer. Researchers at NASA-Lewis [16] found that the presence of water vapor led to the formation of a gaseous $Si(OH)_4$ species via a reaction with the silica layer. The rate of formation of this species, k, and thus the rate at which the SiC (or Si_3N_4) is consumed by its continued oxidation is determined by the expression,

$$k \quad v^{1/2}\, P(H_2O)^2/(P_{total})^{1/2}, \qquad (1)$$

where v is the gas velocity, $P(H_2O)$ is the pressure of the water vapor, and P_{total} is the total pressure.

To address the aforementioned oxidation issues, a study was initiated to examine the effects of high-pressure water vapor upon the long-term reliability of structural ceramics. Utilizing a special high-temperature, high-pressure test facility, silicon nitride and silicon carbide coupons were exposed to a representative gas turbine environment. A typical test exposure consisted of 500 hours at 1204°C and 1.5 atm of water vapor carried in an air environment at 10 atm of total pressure. Following each exposure specimens were weighed, measured, and then sectioned for optical microscopy, scanning electron microscopy (SEM), and x-ray diffraction analysis. The total exposure duration was 1500 h for the silicon nitride and 2000 h for the silicon carbide.

EXPERIMENTAL PROCEDURE

An overview of the high-temperature, high-pressure test facility is shown in Figure 3a. The primary components of the test system are a furnace, ceramic containment tubes, and a gas supply system. The top-loading furnace is capable of 1550°C operation and has external dimensions of about 1.2 m on each side with a hot zone that is approximately 25 cm wide x 41

cm deep x 66 cm high. The top cover of the furnace has six holes. As shown in Figure 3b, each hole accommodates a 8.9 cm OD containment tube (Carborundum's Hexoloy SA). These tubes, which are 1.2 m long, contain the test atmosphere. Approximately 28 cm of the tube extends above the top of the furnace. The tubes are closed at the end that extends into the furnace and the open end has an expanded section to provide a sealing surface and a means to hold the tube. This expanded section accommodates a stainless steel flange that contains fittings so that a pressurized gas mixture can be fed to and removed from the tubes at pressures up to 20.4 atm (300 psia).

An aluminum oxide (hollow tube) specimen holder (Figure 3c) was suspended within each ceramic containment tube. In order to accommodate the specimens to be exposed, regularly spaced slots were machined into the holder. These slots could accept standard flexure bars 3 by 4 by 50 mm. As shown in Figure 3c, larger sized specimens were hung from aluminum oxide pins placed through the machined slots.

The gas supply system permits a measured amount of bottled gas to be combined with a controlled amount of steam to simulate the atmosphere expected in any section of a steam cracker. For these studies, the flow of air, which was used as the carrier gas, was regulated with a mass flow controller. A pneumatically driven metering pump controlled the supply of high-purity distilled water to the evaporator. The amounts of air and distilled water supplied to the system were manually adjusted to the desired proportions (typically to maintain 15% steam). The gas mixture was fed to each of two SA SiC ceramic containment tubes used in this study. The flow rate was 0.3 liters per minute (3 cm/minute linear velocity).

The effluent gas from the ceramic tubes was conducted to a pneumatically driven back-pressure control valve which was controlled through a feedback loop that incorporated a pressure transducer. Water in the effluent was condensed in an air-cooled coil, collected and the volume measured. The volume of the remaining effluent gas was determined using a calibrated flow meter.

One silicon carbide (SA SiC) and 3 silicon nitrides (AS800, SN88, and SN281) were exposed in the high-temperature, high-pressure test facility. The specimen geometry consisted of either flexure bars (3 by 4 by 50 mm) or small dog-bone tensile specimens.

RESULTS

Following the first 500 h exposure, the surfaces of all four materials were light in color (Figure 4) suggesting extensive oxidation. The specific weight and thickness changes measured for all four materials are given in Figures 5 and 6, respectively. The increase in thickness measured for all materials for times up to 1000 h was indicative of the rapid oxidation. Based upon weight and thickness measurements, the SA SiC appeared to exhibit the fastest oxidation. However, the scales formed on the silicon nitride ceramics were less adherent as evidenced by their easy removal through the application of light mechanical pressure.

For exposure times exceeding 1000 h, all materials exhibited a decrease in weight. As discussed below, this behavior could be attributed to the spallation of the oxide scale.

X-ray diffraction was used for phase identification of the intergranular compounds present in the silicon nitrides before testing and after 1500 h of exposure. For the AS800 silicon nitride, the starting material was composed primarily of the H-Phase ($Y_{10}Si_7N_4O_{23}$). During exposure this phase was converted to the J-Phase ($Y_8Si_4N_4O_{14}$). As reported in Reference [17] the J-Phase can lead to instability problems due to its rapid conversion to Y_2SiO_5. Of the two Yb based silicon nitrides, the SN281 exhibited the more stable behavior as reflected by the presence of the $Yb_2Si_2O_7$ phase in both the as-received and exposed specimens. Based upon long-term creep studies [18], $Yb_2Si_2O_7$ is stable

with time. In the case of the SN88, the starting material contained $Yb_4Si_2N_2O_7$, which during exposure transformed to $Yb_2Si_2O_7$. As discussed below, this transformation may have been responsible for changes in the microstructure of intergranular phase.

X-ray diffraction was also used to identify the phases associated with the oxide scale. For all materials examined in this study cristobalite was the primary phase present.

Scanning electron micrographs of polished cross sections of SASiC, AS800, SN88, and SN281 materials are shown in Figures 7 through 10, respectively. The scale on the SiC material consisted of a thick defective (cracked and porous) silica layer (presumably cristobalite) on top of a thin amorphous layer located at the surface of the SiC. Although the total scale thickness increased significantly with time (Fig 7a), the thickness of the amorphous layer stayed constant at 4-6 um. The extensive cracking observed in the outer layer (Fig 7b) may have resulted from the tensile stresses generated by the increase in density accompanying the transformation of the amorphous scale (density = 2.21 g/cm3) to the crystalline silica (density = 2.37 g/cm3). Due to the extensive damage present in the outer silica scale, it is clear that only the amorphous scale acted as an effective barrier to oxygen diffusion. As discussed below this observation explains why parabolic oxidation kinetics were not observed.

As shown in Figure 8 through 10, the scales formed on the silicon nitrides contained numerous cracks and were quite porous, particularly near the oxide surface. Furthermore, these scales consisted of a silica matrix containing isolated regions of the intergranular phase and partially oxidized silicon nitride grains located near the oxidation interface (Figure 11). There was also a tendency for transverse cracks to form within the silicon nitride just below the oxidation interface. The extent of the cracking increased in the order, SN181<SN88<AS800, which corresponds to the decreasing stability of the intergranular phase. In the case of the SN88, the structure of the intergranular phase was altered in the vicinity of the oxidation interface. For example, after 1500 h this affected zone extended 80 µm below the oxidation interface (Figure 12). Based upon the x-ray diffraction results the alteration of the intergranular phase was likely a result of the transformation from $Yb_4Si_2N_2O_7$ to $Yb_2Si_2O_7$.

Because of the problems with scale spallation, the macroscopic thickness and specific weight measurements were not useful for assessing the kinetics of oxidation. In order to overcome this problem, scale thickness of the four materials was measured from polished cross sections using an optical microscope equipped with calibrated x-y stages. The resolution of these measurements was better that 1 µm.

As shown in Figure 13, the oxidation behavior was quite similar for the four materials. The fact that the oxidation kinetics were not parabolic is explained by the highly defective nature of the scale. In the case of the SA SiC, only the amorphous scale could be considered as an oxygen diffusion barrier. The time required to generate the amorphous scale of thickness, X_a (6 µm), is given as

$$t_a = X_a^2/k_P \qquad (2)$$

where k_P is the parabolic rate constant. For $t < t_a$, normal parabolic oxidation kinetics should be followed. However, for $t > t_a$, oxidation should occur at a constant rate given by

$$dX/dt = (k_P\, t_a)^{1/2} \qquad (3)$$

The dashed line in Figure 13 illustrates the best fit of this model to the SA SiC data. The corresponding values for t_a and k_P were 50.4 h and 0.0035 mg^2/cm^4 h. This k_P value compares favorably with the value (0.0037 mg^2/cm^4 h) extrapolated from k_P –P_{H2O} dependence reported in Reference 19.

Based upon the data given in Figure 13, it is clear that the exposure in the high-pressure, high-temperature test facility resulted in extensive oxidation of both the

silicon carbide and silicon nitride ceramics. It is generally accepted that this behavior is due to the presence of high-pressure water vapor. In order to confirm this, the SA SiC was exposed for 100 h in 10 atm air with and without water vapor. Figure 14 illustrates that the oxidation rate was much lower when the water vapor was removed. In this case, the oxygen associated with the air is the only oxidant available.

Recent analysis [20] of a SiC-SiC composite combustor liner utilized in an industrial gas turbine indicates that the oxidation behavior of the SiC seal coat is similar to that obtained in the present investigation. The gas turbine operated for approximately 2300 h at a total pressure of 10 atm. The peak liner temperature was 1150°C. Figure 15 shows the oxide scale present along the internal surfaces of the composite. Note that in this region, the SiC is isolated from the high gas velocities, which can cause volatilization of the scale. The morphology and thickness of this scale are quite similar to those shown in Figure 7.

Finally it must be mentioned that one of the limitations of the high-pressure, high-temperature exposure facility used in this investigation is that the low gas flow velocities do not reflect the conditions in the actual gas turbine combustor. The primary affect of these high velocities is to further limit the steady state value of the oxide thickness (X_a in Equation 2), which will lead to higher rates of SiC recession. Figure 16 compares the SiC seal coat recession rate determined from several SiC-SiC combustor liners with the rates determined in the present study for both SA SiC and a SiC seal coated SiC-SiC composite. In the case of the liners, the time required to breach the seal coat (of known thickness) was indicated from boroscope inspections by the appearance of a light-colored scale on the liner. The rate for the SiC-SiC composite exposed in the high-pressure, high-temperature test facility is approximately 1/3 of that for the liner. That fact that the recession of the SA SiC is even lower may be a result of the differing morphologies of the monolithic material and the seal coat, which is produced by chemical vapor deposition.

SUMMARY

The exposure of silicon carbide and silicon nitride ceramics in a high-pressure, high-temperature test facility resulted in extensive oxidation. In general, the scales that formed were highly defective and thus were ineffective as diffusion barriers to further oxidation. The linear rate of oxide formation is a further consequence of the non-protective nature of the scale. The high rates of scale formation were found to be comparable to those measured for a combustor liner used an industrial gas turbine.

REFERENCES

(1) S. M. Wiederhorn, R. Krause, and D. C. Cranmer, “Tensile Creep Testing of Structural Ceramics,” pp. 273-80 in Proc. Twenty-Fifth Automotive Tech. Development Contractors' Coordination Meeting, P-209 (1991).

(2) W. Luecke, S. M. Wiederhorn, B. J. Hockey, and G. G. Long, Cavity Evolution during Tensile Creep of Si_3N_4," pp. 467-72 in Proceedings of the Materials Research Society Symposium, **Vol. 287**, edited by I-W. Chen, P. F. Becher, M. Mitomo, G. Petzow, and T-S. Yen, 1993.

(3) D. F. Carroll, S. M. Wiederhorn, and D. E. Roberts, "Technique for Tensile Creep Testing of Ceramics," *J. Am. Ceram. Soc.*, 72 (9) 1610-1614 (1989).

(4) W. Luecke and S. M. Wiederhorn, “Interlaboratory Verification of Silicon Nitride Tensile Creep Properties,” submitted to J. Amer. Ceram. Soc. (1) D. Anson, K. S. Ramesh, and M. DeCorso, "Application of Ceramics To Industrial Gas Turbines"; Volume 1 Technology Background; Volume 2 Economics, Market Analysis, and R&D Plan DOE/CE/40878-1&2; Battelle Columbus March 1991.

(5) N. L. Hecht, *Environmental Effects in Toughened Ceramics-Final Report*, UDR-TR-91-15 (February

1991).

(6) N. R. Osborne, G. A. Graves, and M. K. Ferber, " Dynamic Fatigue Testing of Candidate Ceramic Materials for TurbineEngines to Determine Slow-Crack-Growth Parameters," *Journal of Engineering for Gas Turbines and Power*, **119**, 173-8, 1997.

(7) M. K. Ferber and M. G. Jenkins, "Evaluation of the Strength and Creep-Fatigue Behavior of a HIPed Silicon Nitride, "J. *Amer. Ceram. Soc.* , **75**, [9], 2453-62, 1992.

(8) M. K. Ferber, M. G. Jenkins, T. A. Nolan, and R. Yeckley, "Comparison of the Creep and Creep Rupture Performance of Two HIPed Silicon Nitride Ceramics," *J. Amer. Ceram. Soc.* , **77** [3] 657-65, 1994.

(9) M. G. Jenkins, M. K. Ferber and J. A. Salem "Creep and Slow Crack Growth Mechanisms Related to Macroscopic Creep Behaviour of a Silicon Nitride Ceramic at Elevated Temperatures, "pp. 1566-1574 in the Proceedings of the 1992 SEM Spring Conference on Experimental Mechanics, Society of Experimental Mechanics, Bethel, Connecticut (1992).

(10) M. N. Menon, H. T. Fang, D. C. Wu, M. G. Jenkins, M. K. Ferber, K. L. More, C. R. Hubbard, and T. A. Nolan "Creep and Stress Rupture Behavior of an Advanced Silicon Nitride: Part I, Experimental Observations," *J. Amer. Ceram. Soc.* , **77** [5] 1217-1227, 1994.

(11) M. K. Ferber and G. A. Graves, "Long-Term Testing, " pp. 121-38 in the in the Proceedings of the Advanced Turbine Systems Annual Program Review, November 9-11, 1994, DOE/OR-2025.

(12) K. C. Liu and C. R. Brinkman, "Dynamic Tensile Cyclic Fatigue of Si_3N_4," pp. 189-97 in Proc. Twenty-Fifth Automotive Tech. Development Contractors' Coordination Meeting, P-209 (1987).

(13) K. C. Liu and C. R. Brinkman, "Tensile Cyclic Fatigue of Structural Ceramics," pp. 279-284 in Proceedings of the 23rd Automotive Technology Development Contractors' Coordination Meeting, P-165, (1986).

(14) M. A. Karnitz, R. S. Holcomb, I. G. Wright, M. K. Ferber, and E. E. Hoffman, "Materials/Manufacturing Element of the Advanced Turbine System Program," pp. 152-60 in the proceedings of the Advanced Turbine Annual Program Review Meeting Volume I, Morgantown Energy Technology Center, DOE/METC-96, October 1995.

(15) M. G. Jenkins, M. K. Ferber, R. L. Martin, V. T. Jenkins, and V. J. Tennery, Study and Analysis of the Stress State in a Ceramic, Button-Head, Tensile Specimen, ORNL/TM-11767, September, 1991.

(16) E. J. Opila and R. E. Hann, Jr., "Paralinear Oxidation of SiC in Water Vapor, " *J. Am. Ceram. Soc*., **80** 197-205 (1997).

(17) F. F. Lange, S. C. Singhal, and R. C. Kuznicki, "Phase Relations and Stability in the Si3N4-SiO2-Y2O3 Pseudoternary System," *J. Am. Ceram. Soc*., **60** 249-52 (1977).

(18) H. T. Lin, unpublished data, Oak Ridge National Laboratory, March 1998.

(19) E. J. Opila, "Variation of the Oxidation Rate with Water Vapor Pressure *J. Am. Ceram. Soc*., **80** 197-205 (1997).

(20) K. L. More, Peter F. Tortorelli, Mattison K. Ferber, Lawrence R. Walker, James R. Keiser, W. D. Brentnall, N. Miriyala, and Jeffrey R. Price, "Exposure of Ceramics and Ceramic Matrix Composites in Simulated and Actual Combustor Environments," to be presented at ASME TURBO EXPO '99, June 7-10, 1999, Indianapolis, Indiana.

Table 1. Summary of Tensile and Flexure Specimen Matrix Examined in this Program

Material	Supplier	Densification
SA SiC	Carborundum Company Niagara Falls, NY 14302-0832	Sintered
GN10 Si_3N_4	AlliedSignal Ceramic Components Torrance, CA	HIPed
PY6 Si_3N_4	GTE Laboratories, Inc., Waltham, Massachusetts	HIPed
NT154 Si_3N_4	Saint-Gobain/Norton Industrial Ceramics Northboro, MA	HIPed
NT164 Si_3N_4	Saint-Gobain/Norton Industrial Ceramics Northboro, MA	HIPed
SN88 Si_3N_4	NGK Insulators, LTD Nagoya, Japan	Gas Pressure Sintered
AS800 Si_3N_4	AlliedSignal Ceramic Components Torrance, CA	Gas Pressure Sintered
SN253 Si_3N_4	Kyocera Kagashima, Japan	Gas Pressure Sintered
SN281/282 Si_3N_4	Kyocera Kagashima, Japan	Gas Pressure Sintered

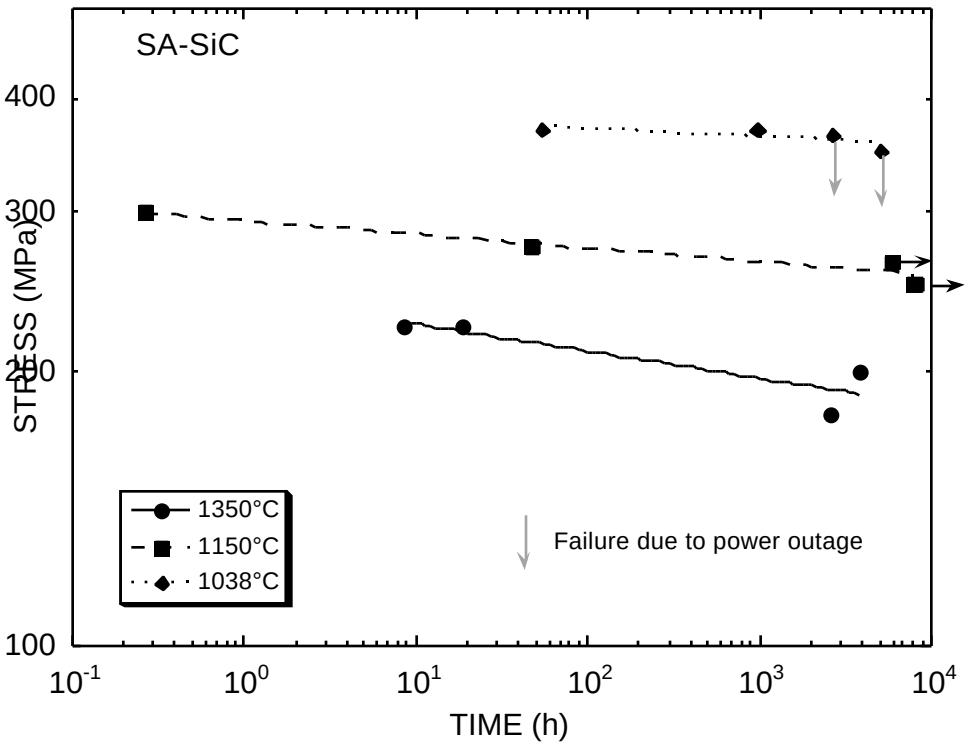

Figure 1. Stress Rupture Data Obtained for SA-SiC.

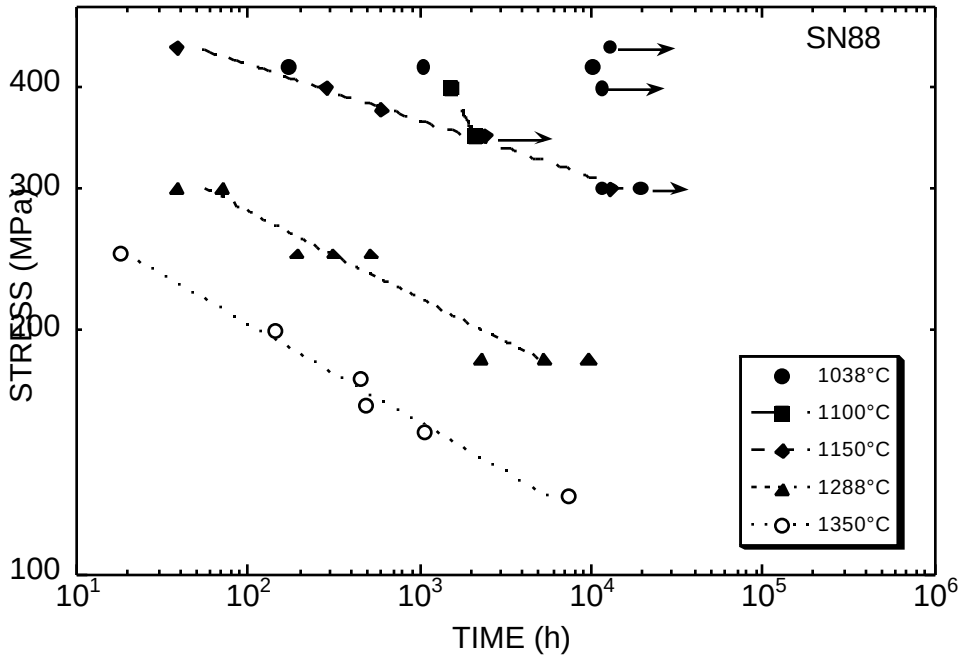

Figure 2. Stress Rupture Data Obtained for SN88 Silicon Nitride.

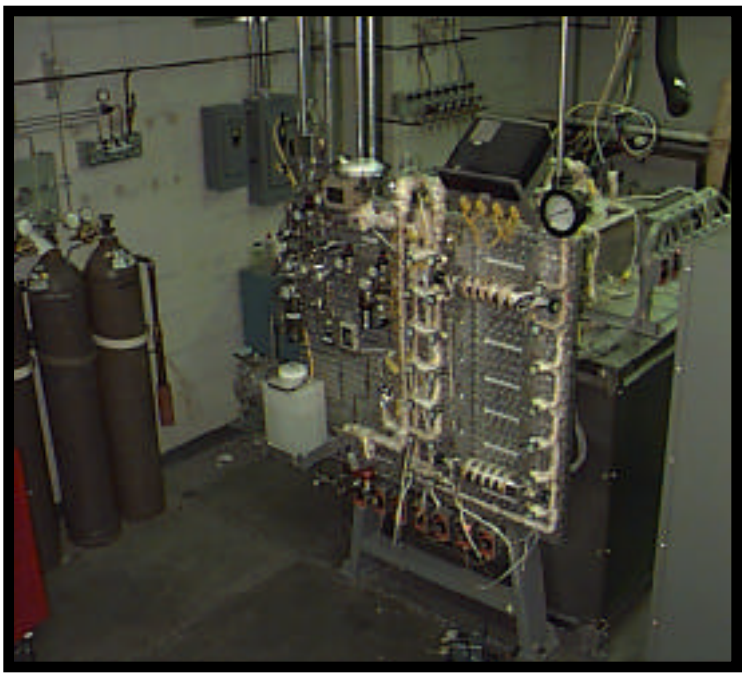

(a)

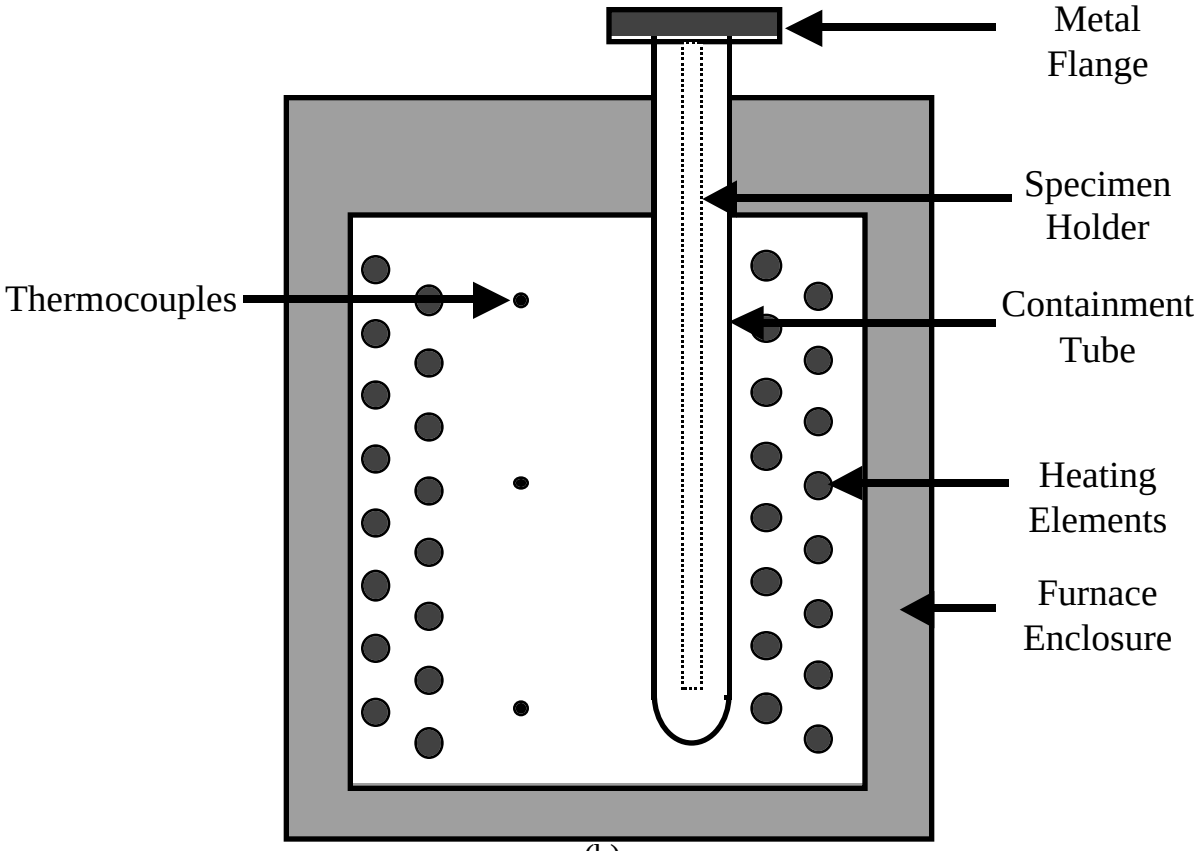
Metal
Flange
Specimen
Holder
Thermocouples
Containment
Tube
Heating
Elements
Furnace
Enclosure

(b)

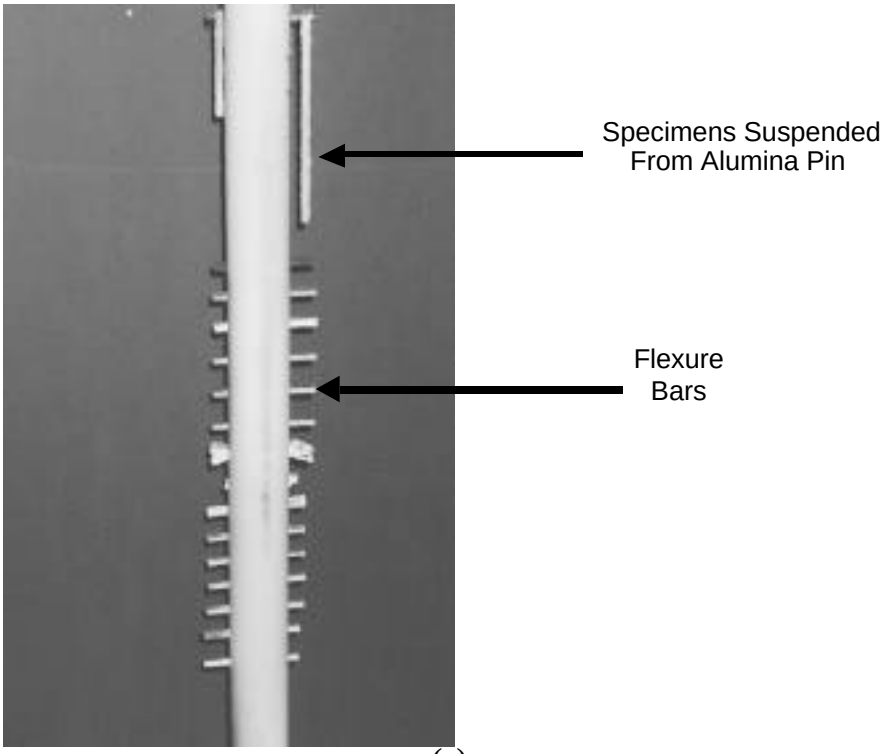

(c)

Figure 3. Key Elements of the High-Temperature, High-Pressure Exposure Facility Including (a) Furnace and Control System, (b) Schematic Drawing of Pressure Containment Tube, and (c) Aluminum Oxide Specimen Holder.

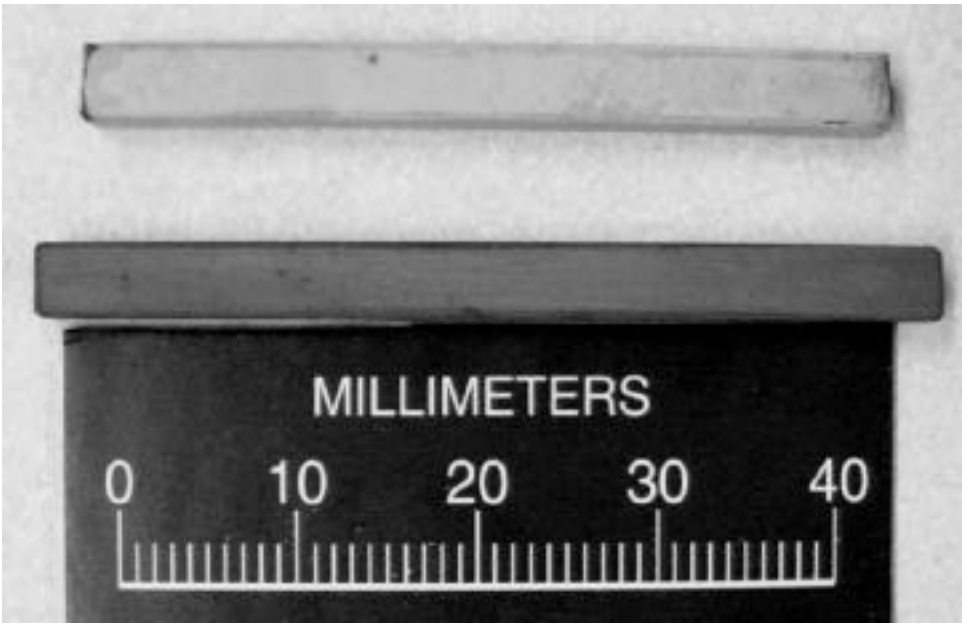

Figure 4. SA SiC Specimen Before (Bottom) and After (Top) First 500 h Exposure.

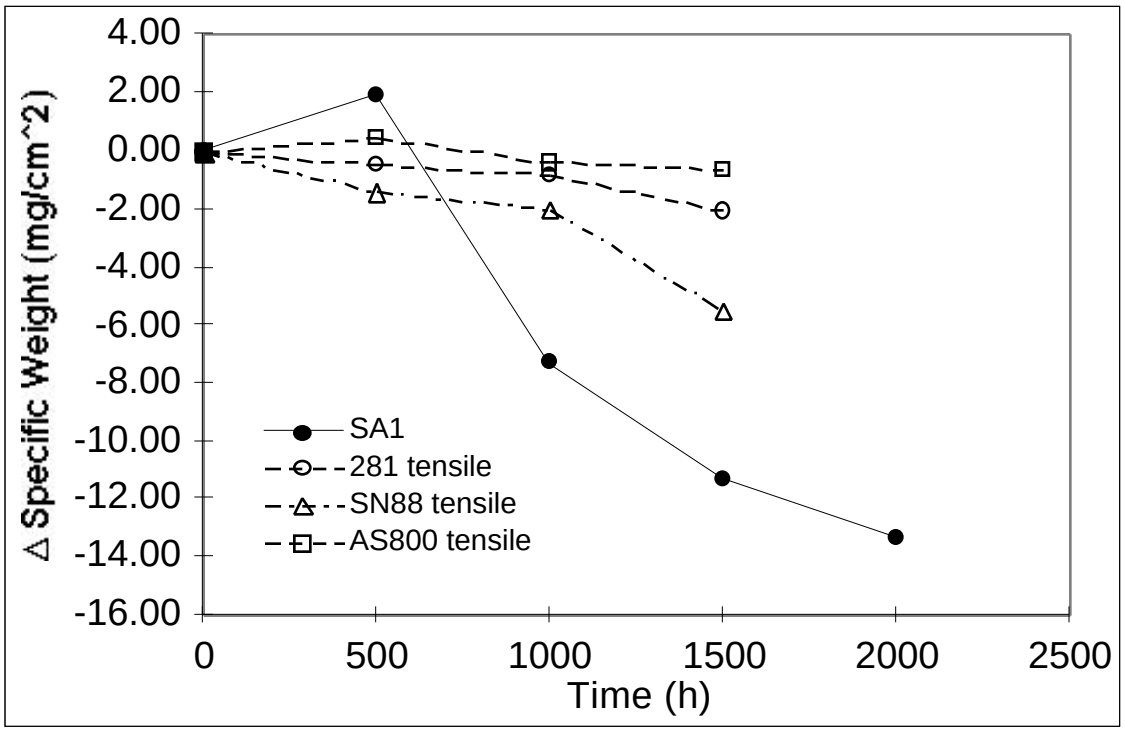

Figure 5. Specific Weight Changes Measured for the Monolithic Specimens.

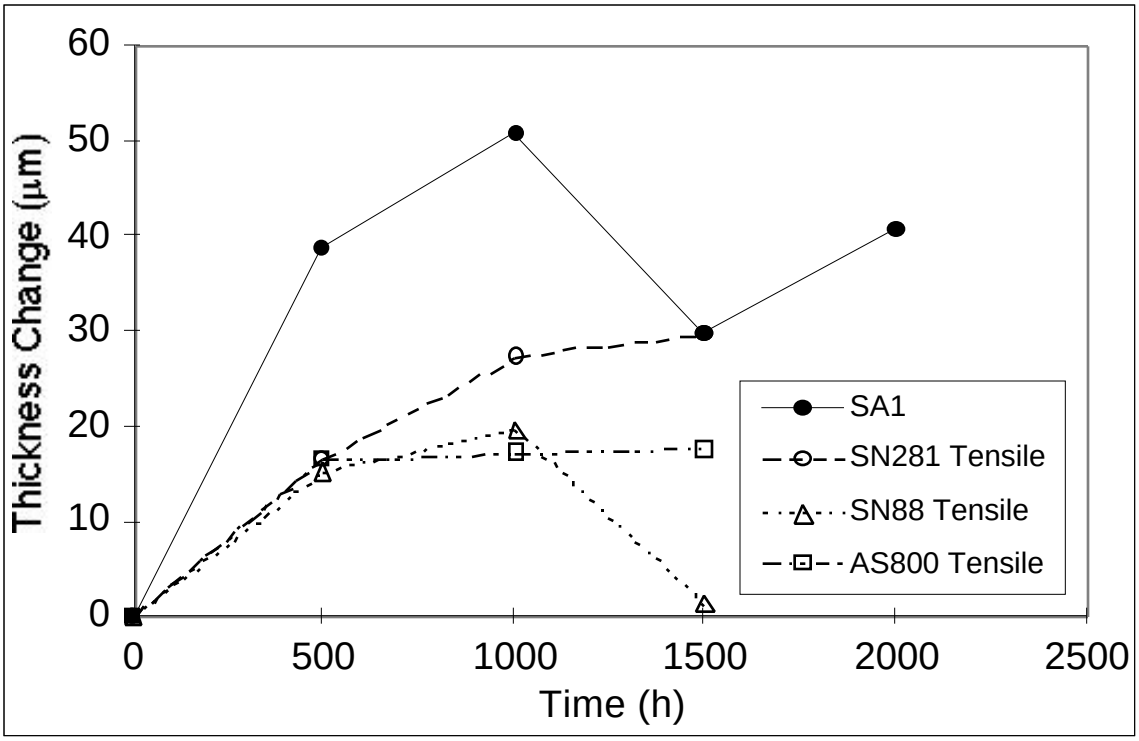

Figure 6. Thickness Changes Measured for the Monolithic Specimens.

(a)

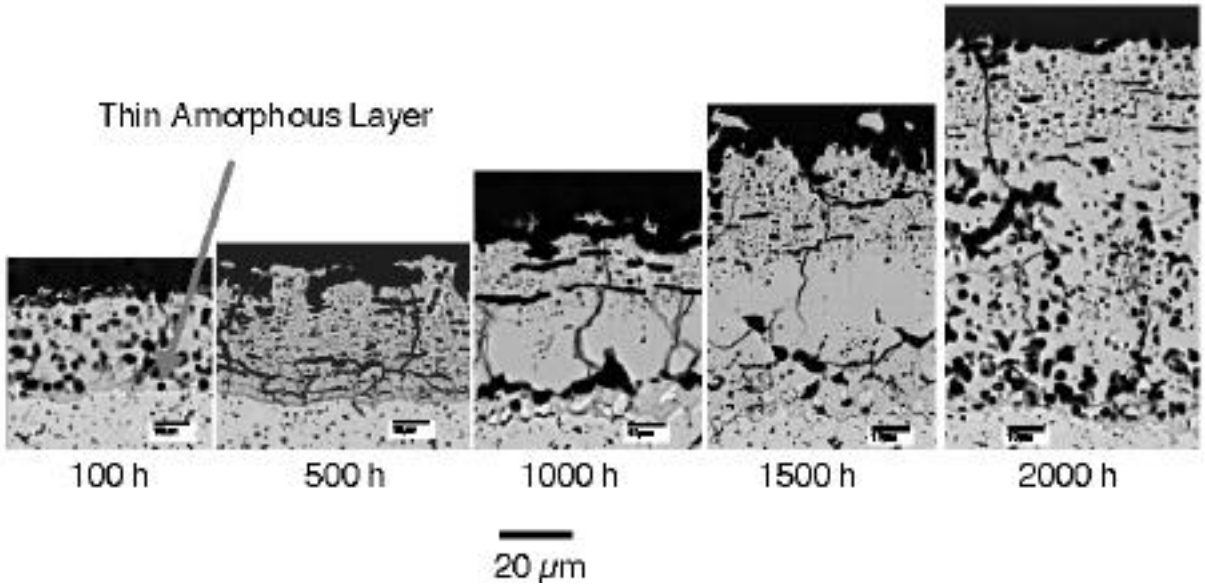

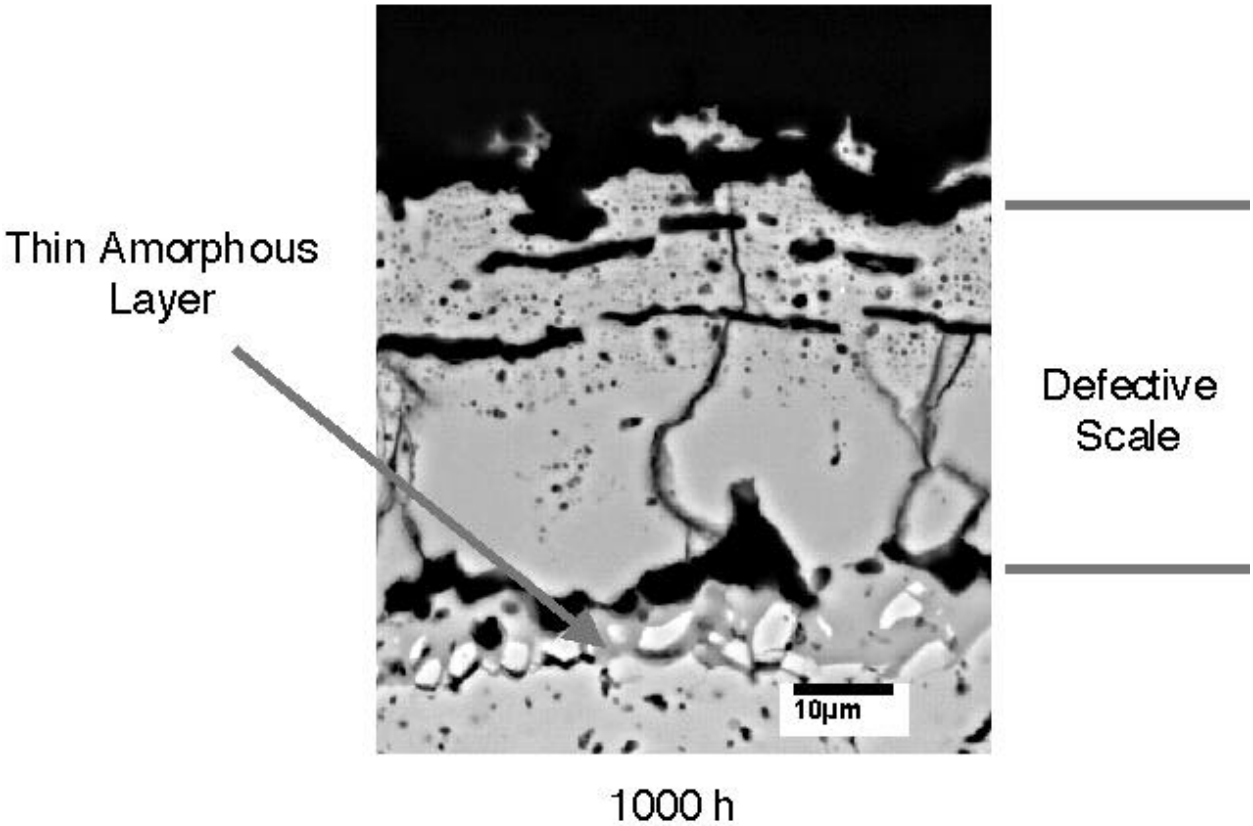

(b)

Figure 7. Polished Cross Sections of SA SiC Showing (a) Evolution of Scale Thickness with Time and (b) Dual Nature of Scale Morphology.

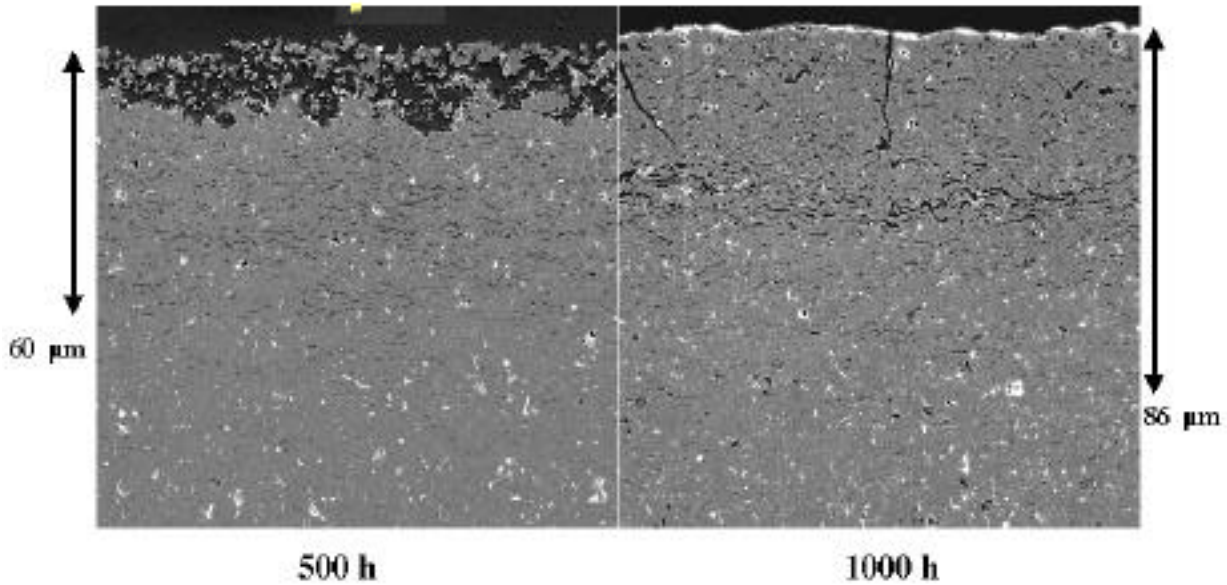

Figure 8. Polished Cross Sections of AS800 Showing Evolution of Scale Thickness with Time.

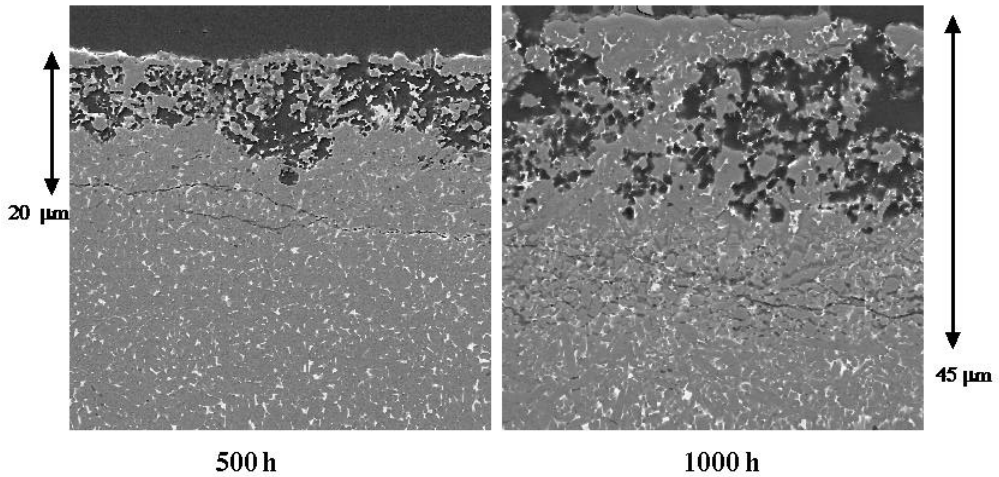

Figure 9. Polished Cross Sections of SN88 Showing Evolution of Scale Thickness with Time.

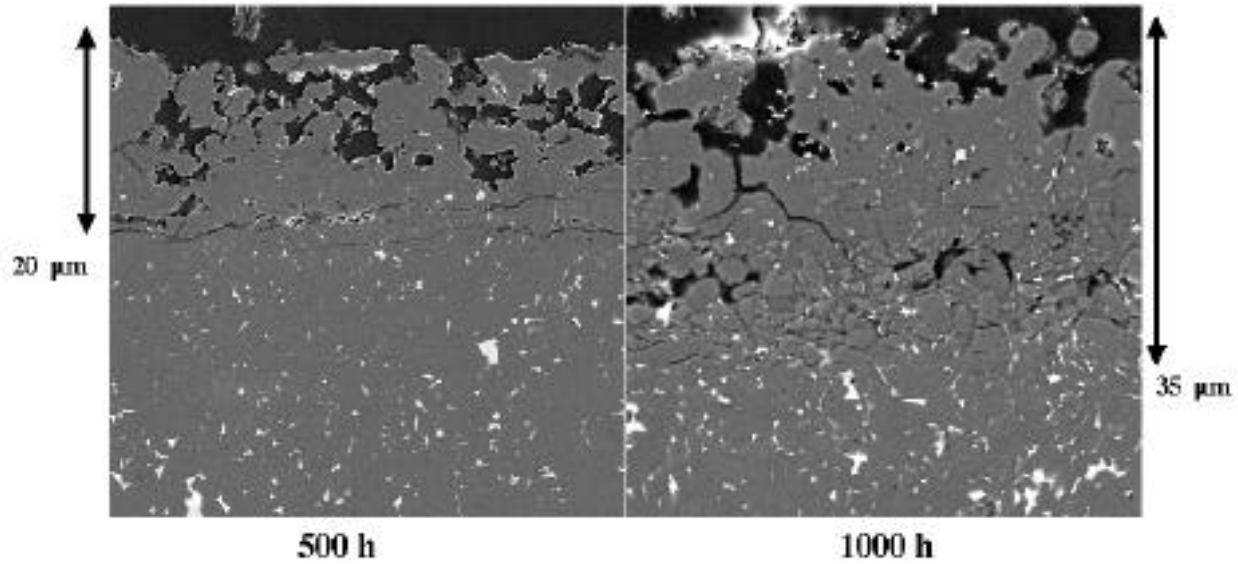

Figure 10. Polished Cross Sections of SN281 Showing Evolution of Scale Thickness with Time.

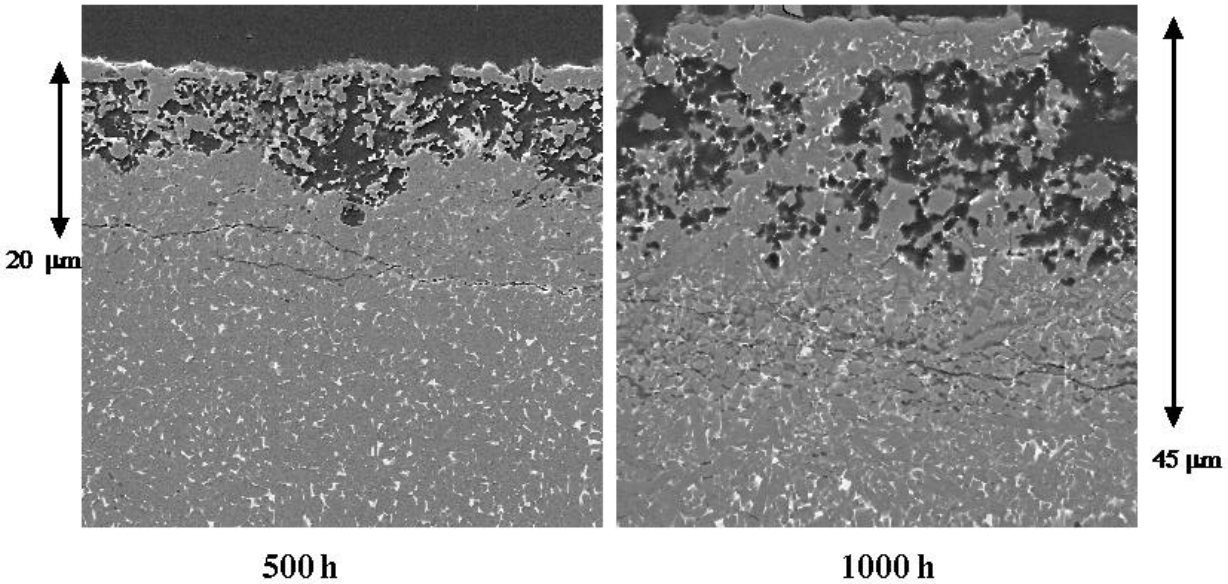

Figure 11. Details of Scale Formed on SN88 after 1000 h.

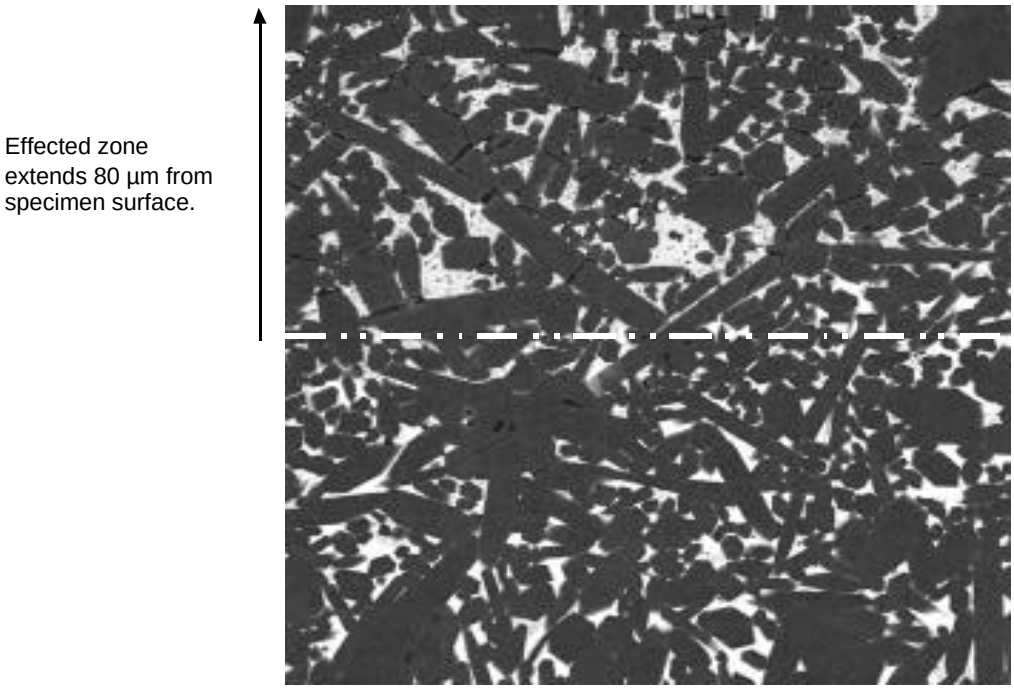

Figure 12. SEM Micrograph Illustrating Physical Modifications in the SN88 Intergranular Phase.

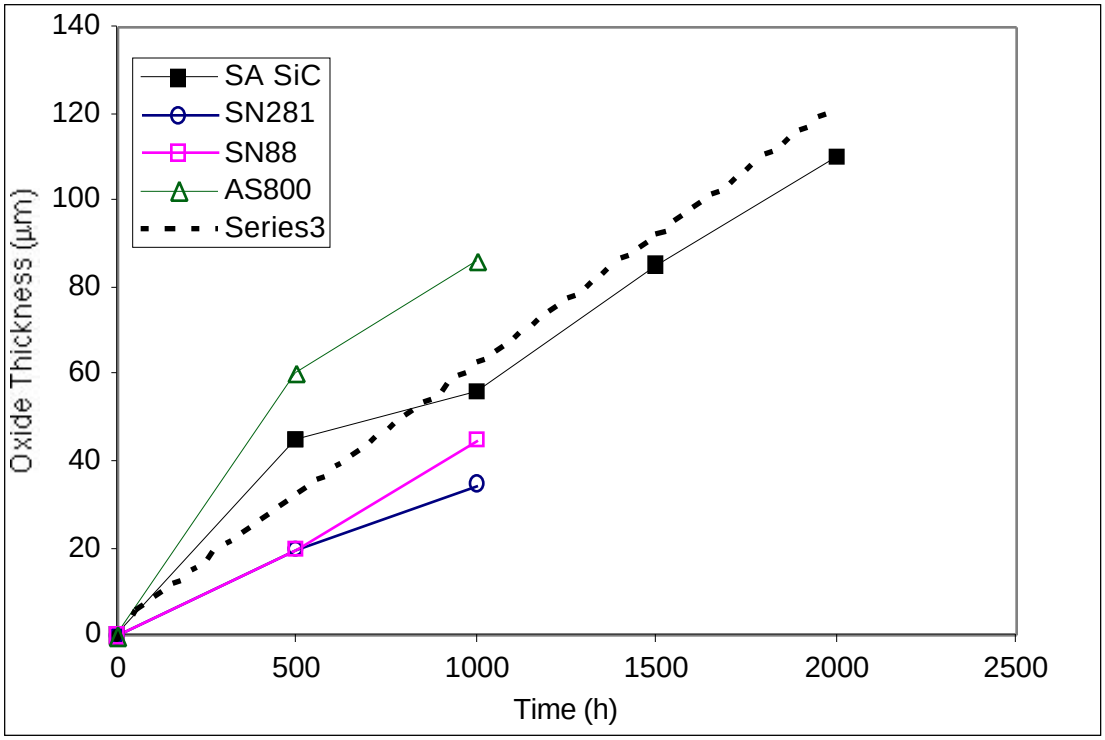

Figure 13. Measured and Predicted (Series 3) Values of Oxide Scale Thickness as a Function of Time.

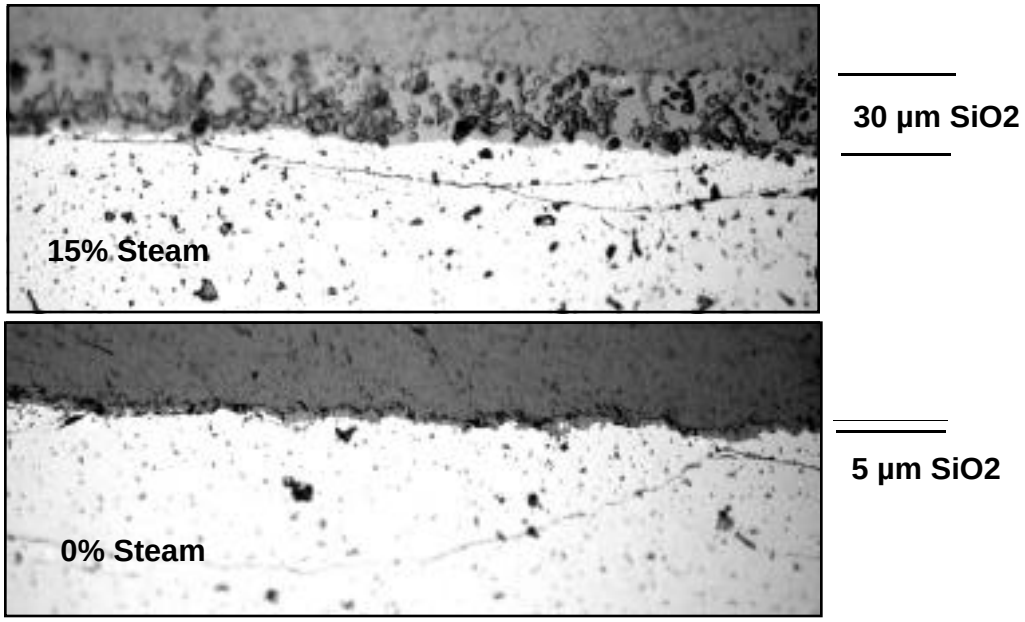

Figure 14. Effect of Waper Vapor Upon the Oxidation Behavior of SA SiC Exposed for 100 h at 1204°C and Air at 10 atm.

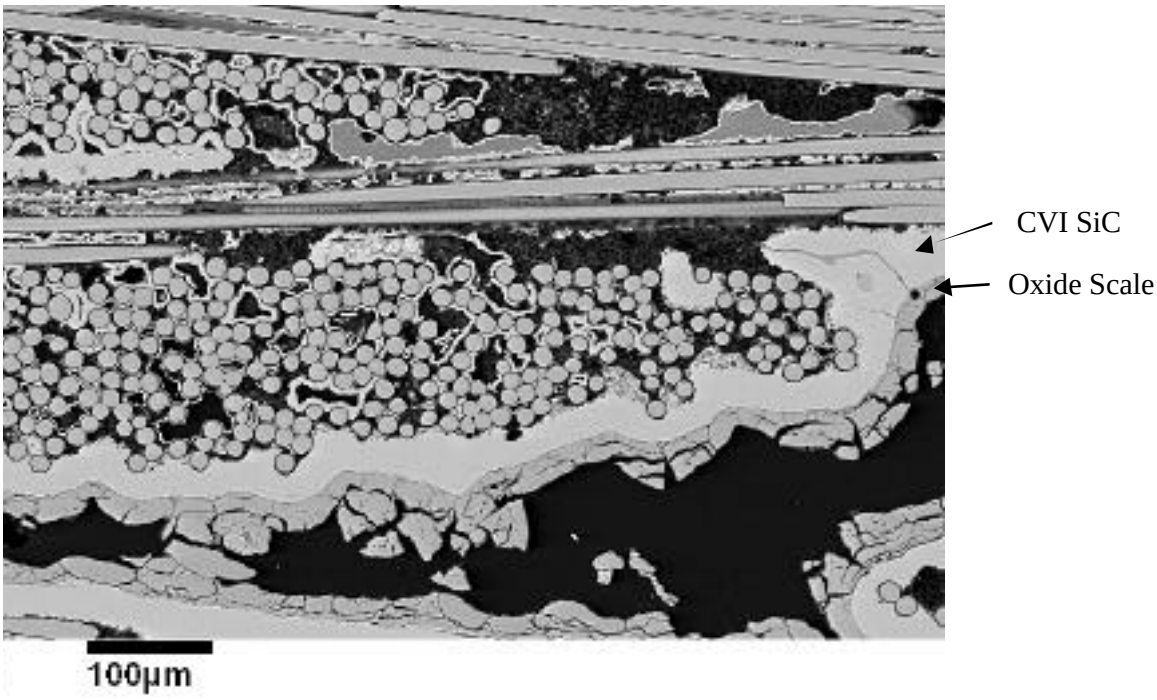

Figure 15. Oxide Scale Present Along the Internal Surfaces of a SiC-SiC Combustor Liner Exposed for 2300 h.

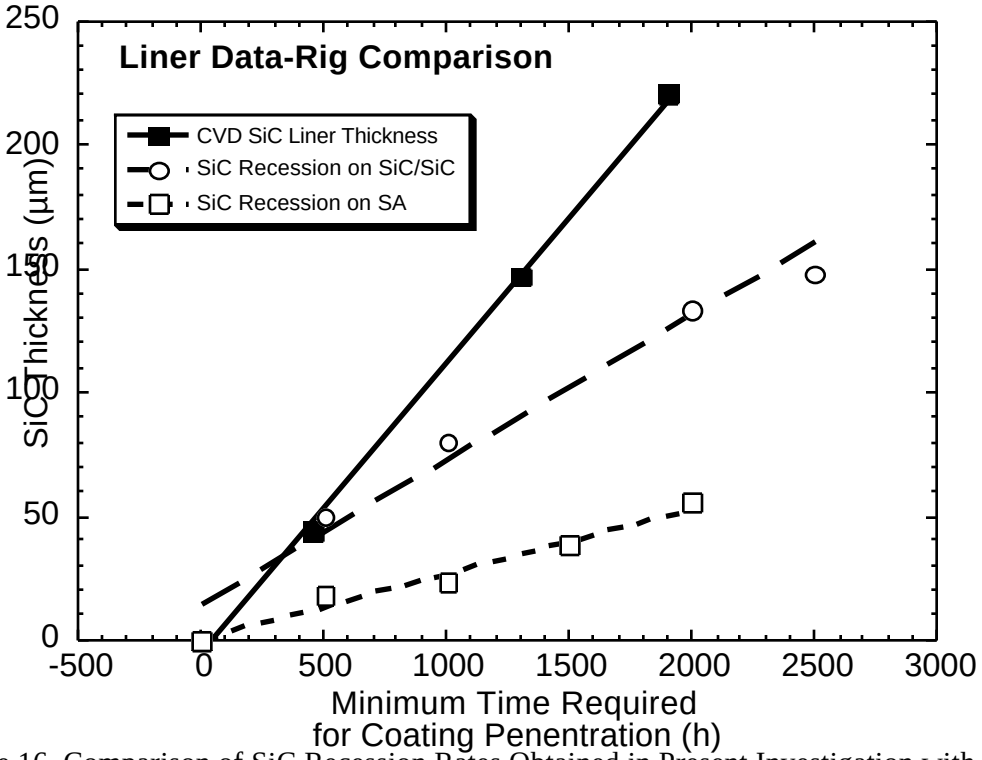

Figure 16. Comparison of SiC Recession Rates Obtained in Present Investigation with Those Measured on Actual SiC-SiC Combustor Liners.